Static Light Scattering of Concentrated Silica Dispersions in Apolar Solvents

A. K. VAN HELDEN AND A. VRIJ

Van't Hoff Laboratory for Physical and Colloid Chemistry, Transitorium III, Padualaan 8, 3584 CH Utrecht, The Netherlands

Organophilic silica dispersions, containing spherical monodisperse particles up to concentrations of 80% (w/v) of silica, were studied with the (static) light-scattering method. Cyclohexane and chloroform were chosen as solvents in order to minimize the scattering intensity. The results were interpreted with fluid-state theories. In a large range of silica concentrations the osmotic compressibility as well as the scattering at finite angles could be described rather well with hard-sphere interactions. The hard-sphere radius was rather close to the hydrodynamic radius of the particle. At the highest particle concentrations the scattering intensity sharply increases for small scattering angles. This is attributed to formation of large dense clusters of primary particles.

I. INTRODUCTION

An understanding of interparticle interaction and stability in *concentrated* colloidal dispersions is of much interest in theoretical and applied colloid science. An attractive approach comprises application of concepts and techniques from the field of molecular (monoatomic) fluids. The colloidal particles play the role of "supramolecules" dispersed in a "structureless" background of low-molecular-weight solvent. Recently this approach has been used in studies on the light scattering of aqueous (1, 2) and nonaqueous (3) latex dispersions and of microemulsions (4). Also sedimentation equilibrium and osmotic pressure measurements of hemoglobin solutions were interpreted in this manner (5).

In this paper we shall report on (static) light-scattering experiments on concentrated silica dispersions in cyclohexane and chloroform.

An advantage of the light-scattering method is that it can be used to determine (osmotic) compressibilities in the whole concentration region from very dilute to very concentrated dispersions, the reason being that with increasing particle concentration the scattered intensity first increases and often attains a maximum value, after which it decreases again. A direct osmotic pressure measurement is often too insensitive at small particle concentrations. A drawback of the light-scattering method, however, is the limited choice of solvents, because the scattering power of the system must be minimized in order to avoid multiple scattering.

The silica particles which are used in our study consist of a spherical silica core coated with relatively short aliphatic chains (18 carbon atoms). These organophilic silica dispersions are a promising alternative to other model colloids, because they can be studied in a large concentration range. Cyclohexane and chloroform are chosen because of appropriate refractive indices and good solvent properties. In these apolar solvents we expect electrostatic forces to be of minor importance and van der Waals forces are probably also small because the refractive indices of particles

and solvent are nearly equal. The main interaction force would then be steric in nature and because the coating layer of the silica is thin, the repulsion will also be steep. In view of this we expect the dispersion to behave almost as a hard-sphere system, which is of interest because this system is relatively simple and theoretical results are known.

In Section II some basic light scattering- and fluid-state-theory equations are recalled. Special attention is paid to the hard-sphere fluid (Percus–Yevick approximation). The influence of hard-sphere interaction on the angular dependence of scattered light at low K is shown explicitly. Also earlier reported results of (a) hard convex, (b) polydisperse, and (c) clustered systems are discussed, because they are relevant to colloidal dispersions. Materials and methods are discussed in Section III and particle characterization in Section IV. Light scattering in dilute and concentrated dispersions is presented (Section V) and interpreted (Section VI). Section VII deals with large clusters appearing at high concentrations. In Section VIII discussion of results and conclusions are presented.

II. THEORETICAL

1. LIGHT SCATTERING

The light-scattering theory for spherically symmetric particles in the Rayleigh–Gans–Debye (RGD) approximation is well known (6). For unpolarized light the normalized excess scattering per unit volume (Rayleigh ratio) of a dispersion over that of the solvent is given by

$$R(K) = (1 + \cos^2 \theta)\mathcal{K}cMP(K)S(K). \quad \text{[II1]}$$

Here $K = (4\pi n/\lambda_0) \sin (\theta/2)$ is the scattering wave vector, θ is the scattering angle, M is the particle molar mass, $c = \rho M/N_A$ is the weight concentration with ρ the particle number density, N_A is Avogadro's number, and

$$\mathcal{K} = 2\pi^2 n^2 (dn/dc)^2 (\lambda_0^4 N_A)^{-1} \quad \text{[II2]}$$

with n the refractive index of the dispersion and λ_0 the wavelength of the incident light *in vacuo*.

$P(K)$ is the intraparticle structure factor. In the Guinier approximation (7) it has the form

$$P(K) = e^{-(1/3)K^2R_g^2}, \quad \text{[II3]}$$

where R_g is the optical radius of gyration of the particle. For small K it becomes

$$P(K) = 1 - (1/3)K^2R_g^2 + \cdots. \quad \text{[II4]}$$

$S(K)$ is the structure factor, which expresses the influence of particle–particle interactions on the scattering. For a spherically symmetric interaction it can be written as (8)

$$S(K) = 1 + \rho\bar{h}(K) \quad \text{[II5]}$$

with

$$\bar{h}(K) = 4\pi \int_0^\infty r^2 h(r)(Kr)^{-1} \sin Kr dr. \quad \text{[II6]}$$

Here $h(r)$ is the total correlation function which is equal to the radial distribution function $g(r)$ minus one. $g(r)$ expresses the probability of finding a particle at a distance r from a given particle. For $K \to 0$, $S(K)$ is related to the osmotic pressure Π by the compressibility relation (9)

$$S(0) = k_B T[\partial\Pi/\partial\rho]^{-1}. \quad \text{[II7]}$$

Then the scattering intensity becomes

$$R(K \to 0) = \frac{2\mathcal{K}cRT}{\partial\Pi/\partial c} . \quad \text{[II8]}$$

Further, k_B is the Boltzmann constant, $R = k_B N_A$ is the gas constant, and T is the absolute temperature.

For low concentrations $\partial\Pi/\partial c$ can be expressed with a virial series,

$$\frac{1}{RT} \frac{\partial\Pi}{\partial c} = \frac{1}{M} (1 + 2A_2c + \cdots), \quad \text{[II9]}$$

which in combination with Eq. [II8] leads to the familiar result for dilute systems.

2. STRUCTURE FACTOR: HARD SPHERES

It is known that in concentrated systems hard repulsive interactions dominate the structural features of a fluid. The prototype hard repulsion for spherically symmetric interactions is the hard-sphere potential,

$$U(r) = \begin{cases} \infty & r < \sigma \\ 0 & r \geqslant \sigma, \end{cases} \quad [II10]$$

where σ is the hard-sphere diameter. Even for this simple pair potential no exact method exists to calculate $h(r)$ and $S(K)$. Several approximate theories have been developed and tested with computer simulations (10). Well known is the Percus–Yevick (PY) theory (11). It is very successful for hard repulsions and has the important feature that it gives an *analytic* solution for the hard-sphere potential (12).

It has the following form:

$$\tilde{h}(K) = \frac{\tilde{c}(K)}{1 - \rho\tilde{c}(K)}, \quad [II11]$$

with

$$\tilde{c}(K) = 4\pi \int_0^\sigma r^2 c(r)(Kr)^{-1} \sin Kr\, dr, \quad [II12]$$

where $c(r)$ is an auxiliary function: the so-called direct correlation function. In the PY approximation,

$$c_{PY}(r) = \alpha + \beta(r/\sigma) + \gamma(r/\sigma)^3,$$
$$0 \leqslant r \leqslant \sigma. \quad [II13]$$

The coefficients α, β, and γ are simple functions of the volume fraction, ϕ, of the hard spheres, given by:

$$\phi = \frac{1}{6}\pi\sigma^3\rho. \quad [II14]$$

For $K = 0$, it is found that (8)

$$S(K = 0) = k_B T\left(\frac{\partial\rho}{\partial\Pi}\right)_{PY}$$
$$= \frac{(1 - \phi)^4}{(1 + 2\phi)^2}. \quad [II15]$$

We also need $S(K)$ for small but finite K. A series expansion of $\sin Kr$ under the integral [II12] yields

$$\frac{S(K = 0)}{S(K)} = 1 - \chi(\phi)K^2\sigma^2 + \cdots, \quad [II16]$$

with

$$\chi_{PY}(\phi) = \frac{\frac{4}{5}\phi - \frac{11}{20}\phi^2 + \frac{1}{5}\phi^3}{(1 + 2\phi)^2}. \quad [II17]$$

Expression [II15] is known as the compressibility version of the PY theory. It yields somewhat too high values of $\partial\Pi/\partial\rho$ compared with machine calculations: e.g., 8% for $\phi = 0.4$. Carnahan and Starling (CS) (13) proposed a semiempirical extension, which can be written as

$$S^{-1}(K = 0) = \frac{1}{k_B T}\left(\frac{\partial\Pi}{\partial\rho}\right)_{CS}$$
$$= \frac{(1 + 2\phi)^2 - \phi^3(4 - \phi)}{(1 - \phi)^4}. \quad [II18]$$

It agrees within graphical accuracy with computer simulations in the fluid branch of $\Pi(\rho)$.

Both [II15] and [II18] are exact up to and including terms in ϕ^2,

$$\frac{1}{k_B T}\frac{\partial\Pi}{\partial\rho} = 1 + 8\phi + 30\phi^2 + \cdots. \quad [II19]$$

Sharma and Sharma (14) introduced a semiempirical extension of the CS equation to obtain $\tilde{c}(K)$. This leads to a function $\chi(\phi)$ that deviates less than 1% from Eq. [II17]. In the discussion of our experimental results we will use Eq. [II16] in conjunction with the Eqs. [II18] and [II17].

3. NONSPHERICITY AND POLYDISPERSITY

Colloidal particles are neither completely spherical nor completely monodisperse. It is therefore necessary to estimate the influence of these effects on $S(K)$.

(a) Nonsphericity

No closed expressions for $S(K)$ are known for nonspherical particles as far as we know. For $K = 0$, however, one may use equations for Π as given by the so-called scaled particle theory (SPT). For hard, convex particles with arbitrary shape, e.g., ellipsoids, tetrahedrons, cubes, and cylinders (15, 16), the following simple equation is found:

$$\frac{1}{k_{\mathrm{B}}T}\left(\frac{\partial \Pi}{\partial \rho}\right)_{\mathrm{SPT}} = \frac{[1 + (3k - 1)\phi]^2}{(1 - \phi)^4}, \quad [\mathrm{II}20]$$

where $\phi = V\rho$, $k = \bar{R}S/3V$ with $\bar{R}$ the radius averaged over all orientations, S the surface area, and V the volume of the particles. Note that for spheres ($k = 1$) this equation is identical to the PY equation [II15]. Equation [II20] is also quite good for dumbbells (17) if one takes $k \sim 1.6$.

A CS type of correction (18) and computer experiments (19, 20) are also described in the literature. Equation [II20] predicts an increased $\partial\Pi/\partial\rho$ and thus a decreased $S(0)$ for deviations from the spherical shape. Quantitative results are discussed in Section II.4.

(b) Polydispersity

The effect of polydispersity in size and scattering power is known for hard spheres in the PY approximation (21). For $K \to 0$ one finds

$$S(0) = (1 - \phi)^4(1 + 2\phi)^{-2}\Omega(\phi) \quad [\mathrm{II}21]$$

with

$$\Omega(\phi) = 1 + 6\phi(1 - \phi)^{-1}$$
$$\times [1 - \langle\sigma^4\rangle\langle\sigma^5\rangle\langle\sigma^3\rangle^{-1}\langle\sigma^6\rangle^{-1}]$$
$$+ 9\phi^2(1 - \phi)^{-2}[1 - 2\langle\sigma^4\rangle\langle\sigma^5\rangle\langle\sigma^3\rangle^{-1}\langle\sigma^6\rangle^{-1}$$
$$+ \langle\sigma^4\rangle^3\langle\sigma^3\rangle^{-2}\langle\sigma^6\rangle^{-1}], \quad [\mathrm{II}22]$$

where $\langle \rangle$ means number average and $dn/d\rho_i$ is taken proportional to σ_i^3. Polydispersity tends to increase $S(0)$.

4. NUMERICAL RESULTS; CONCLUDING REMARKS

Some calculated hard-particle results are shown in Fig. 1. Because all the scattering equations contain the strongly concentration-dependent factor $(1 - \phi)^4$, this factor is extracted from $\partial\Pi/\partial\rho$.

In Fig. 1 one observes that the CS equation for hard spheres yields slightly lower values than the PY equation, as already mentioned.

The correction for particle size polydispersity is calculated with the actual size distribution of our sample (see Section IV). The curve is lower than the monodisperse PY curve.

The opposite case is found for deviations of the particle shape from the perfect sphere. Any nonspherical, hard interaction leads to an increase in $\partial\Pi/\partial\rho$ compared with the hard sphere. Results are shown for $k = 1.2$, which corresponds for instance with the hard prolate spherocylinders treated by Few et al. (19). We also presented the case of prolate ellipsoids with an axis ratio $(a_1/b_1) = 1.5$. Isihara and Hayashida (22) and Kihara (23) presented a method to calculate k for hard prolate ellipsoids as a function of the eccentricity, $e^2 = (a_1^2 - b_1^2)/a_1^2$. We used the result $k = 1 + (4/45)(e^4 + e^6)$, which is valid for small e, to calculate that $k = 1.059$ for $a_1/b_1 = 1.5$. One may conclude that the correction for the particles being ellipsoids rather than spheres is small and tends to compensate polydispersity effects.

$\partial\Pi/\partial\rho$ of the hard dumbbell (DB) shows an appreciable deviation which increases very rapidly with the volume concentration. In Fig. 1 the approximation of Nezbeda's result (17) is shown. Intuitively one expects for high volume fractions that $(\partial\Pi/\partial\phi)_{\mathrm{DB}} \simeq (\partial\Pi/\partial\phi)_{\mathrm{HS}}$, i.e., $(\partial\Pi/\partial\rho)_{\mathrm{DB}} \simeq 2(\partial\Pi/\partial\rho)_{\mathrm{HS}}$ since $\rho_{\mathrm{DB}} = 0.5\rho_{\mathrm{HS}}$. Multiplying the ordinate for the hard-sphere case by $2^{1/2}$ yields the line indicated in Fig. 1 with (x). It can be seen that indeed for $\phi \simeq 0.4$ equal values are found.
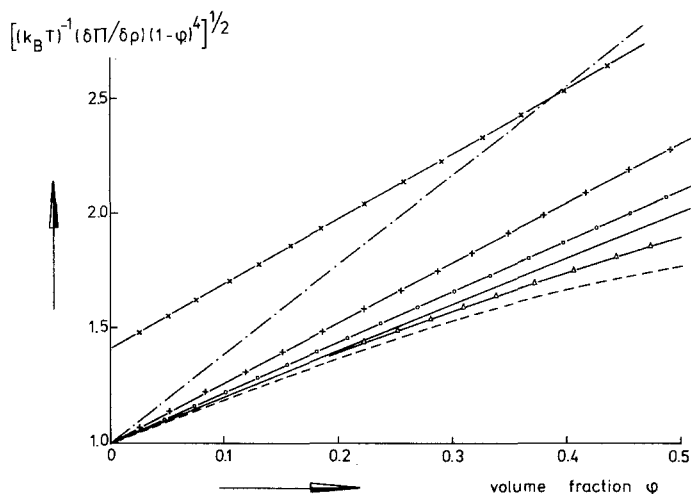
FIG. 1. Theoretical results of molecular hard-fluid theories: (———) PY theory; ($\triangle$) CS equation; (+) reciprocal compressibility of particles with $k = 1.2$, for instance prolate spherocylinders with length to thickness ratio 2; ($\bigcirc$) idem for particles with $k = 1.059$; (-----) $[S(0)]^{-1}$ according to Eq. [II21] with the experimental value (13%) for the standard deviation; (– · –) Nezbeda's result approximated according to Eq. [II20]; (×) explanation is given in text.

Finally we want to make a brief remark on attractive interactions. The theory of fluids with an interaction potential different from the hard-sphere $U(r)$, Eq. [II10], is complicated. We will only briefly mention here a semiempirical approach, sufficient for our further discussions which was used by Agterof $et\ al.$ (4) to include a van der Waals attractive term. They write for the reciprocal compressibility

$(k_B T)^{-1}(\partial \Pi/\partial \rho)$

$\qquad = (k_B T)^{-1}(\partial \Pi/\partial \rho)_{CS} - \epsilon\phi,$ [II23]

where ϵ (>0) is a parameter describing the attractive force and $(k_B T)^{-1}(\partial \Pi/\partial \rho)_{CS}$ is given by Eq. [II18].

III. MATERIALS AND METHODS

Lyophilic silica particles were prepared in two steps. A silica dispersion in ethanol (alcosol) was prepared according to the method of Stöber $et\ al.$ (24). The concentrations of reagents were 0.5 M NH_3, 1.3 M H_2O, and 0.14 M ethylorthosilicate. The reaction was carried out at ambient tem-

perature. Then stearyl alcohol was added to the alcosol and ammonia and ethanol were distilled off. The reaction of stearyl alcohol with the silica surface was carried out according to the method of Iler (25) at 180°C. The product (coded S_3) was purified from excess stearyl alcohol by leading nitrogen over the heated melt (180°C), thus carrying the stearyl alcohol vapor away. When most of the stearyl alcohol was removed the silica was dispersed in cyclohexane and after centrifugation the supernatant was discarded. For further details of the preparation of lyophilic silica dispersions we refer to a forthcoming paper (26).

Light-scattering measurements were carried out with three series: A, B, and C. In series A the silica was dispersed in cyclohexane after one centrifugation. In series B the silica was centrifuged three times and then dispersed in cyclohexane. In series C the silica was centrifuged three times and after drying redispersed in chloroform.

The light-scattering measurements were performed with a Fica 50 light-scattering photometer (Société Francaise d'Instruments de Controle et d'Analyse). As a

scattering standard pure benzene was used ($R_{90} = 15.8 \times 10^{-6}$ cm^{-1} at $\lambda_0 = 546$ nm, and 45.6×10^{-6} cm^{-1} at $\lambda_0 = 436$ nm). The experiments were carried out with the 546- and 436-nm (unpolarized) lines of a Philips CS 100 W/Z mercury arc lamp, at temperatures between 24.4 and 27.0°C.

At high scattering intensities attenuation of the primary and scattered beams becomes important. We assumed multiple scattering to be of minor importance. The attenuation correction was applied according to the method of Putzeys and Dory (27), which comprises an iteration procedure with $R_{90} = R'_{90} \exp(\tau l)$, where the turbidity $\tau = (16\pi/3)R_{90}$. R_{90} is the Rayleigh ratio observed at $\theta = 90°$. For the highest scattering intensities the correction is 27%.

Transmission electron microscope measurements were performed with a Philips EM 301 apparatus. Carrier grids covered with carbon-coated Parlodion films were dipped in a dilute dispersion and electron micrographs were taken of the particles retained on the film.

Light-scattering fluctuation spectroscopy was performed with a laboratory-built instrument containing a double-walled thermostated sample holder ($25.0 \pm 0.1°C$). The 514.5-nm line of an Ar-ion laser (Spectra Physics Model 165) was used and the light was detected by an EMT 9558 photon multiplier. The correlation function was determined with a Saicor–Honeywell 42A correlator, with a photon-counting option. The correlation functions were analyzed numerically.

Sedimentation velocity experiments were carried out in a Beckman–Spinco Model E analytical ultracentrifuge using a 12-mm standard single-sector cell and an AN-D rotor at temperatures between 23.1 and 23.5°C. A series of consecutive pictures was taken of the Schlieren image of the samples. The rotor speed was 6000 rpm.

Density measurements were conducted at 25.10°C with a Precision Density Meter DMA 02C (Anton Paar KG, Austria).

IV. PARTICLE CHARACTERIZATION

1. Electron Microscopy

Electron micrographs were taken to determine the shape, size, and size distribution of the particles (Fig. 2). The shape of the particles is irregular. This, however, might be caused by the crowding of particles due to capillary forces upon evaporation of the solvent. In solution the particles are probably more spherical. The size of the particles was determined by measuring $a_{EM} \equiv (a_1 b_1)^{1/2}$, a_1 and b_1 being the long and short axes of the particle. We found a number-average radius of 16.5 nm. Compared with the hydrodynamic radius (see next section), this is quite low. We think that this discrepancy is the result of particle shrinkage as a result of radiation (26). The size distribution is shown in Fig. 3. The standard deviation is 13%. For a sample very similar to S_3 the mean ratio $(a_1 b_1)$ was 1.3 ± 0.2.

2. Light-Scattering Fluctuation Spectroscopy

Light-scattering fluctuation spectroscopy was performed with dilute S_3 dispersions in cyclohexane, chloroform, and n-heptane. The autocorrelation function, $F(K,\tau)$, was determined for angles, $15° \leq \theta \leq 135°$. According to the theory, as described in detail by Berne and Pecora (28), the autocorrelation function for the fluctuations in the scattered intensity of noninteracting particles is given by

$$F(K,\tau) \sim \exp(-\zeta\tau) \qquad [\text{IV1}]$$

with $\zeta = 2D_0 K^2$. Here D_0 is the diffusion coefficient and τ is the correlation time. For each K the logarithm of the autocorrelation function was fitted with a quadratic function in τ, and D_0 was found according to the usual cumulant method. For dilute dispersions the hydrodynamic radius, a_D, is related to D_0 by the Stokes–Einstein law,

$$D_0 = k_B T/(6\pi\eta_0 a_D), \qquad [\text{IV2}]$$

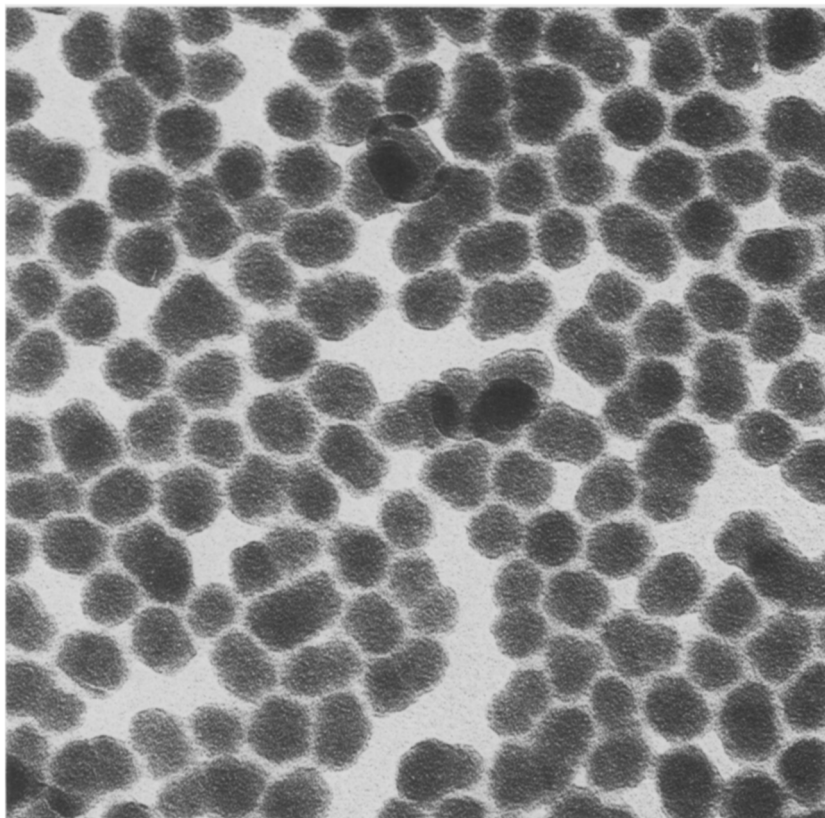where η_0 is the viscosity of the solvent (29).

Fig. 2. Electron micrograph of sample S_3.

The diffusion coefficient appeared to be slightly dependent on the scattering angle, θ. In Table I average D_0 values are listed, which are determined by taking the best linear fit in a ζ versus K^2 plot. As a result of this averaging, D_0 is mainly determined by the scattering at higher angles. For both solvents D_0 at $\theta = 15°$ is approximately 10% smaller than the mean value. The hydrodynamic radius, a_D, is calculated with Eq. [IV2]. For the different solvents almost the same value for a_D was found.

3. Ultracentrifuge Experiments

Measurements were carried out in cyclohexane (30) and also in n-heptane in order to increase the difference in refractive index between particle and solvent (for n-heptane $\Delta n = 0.06$). The sedimentation constant

was extrapolated to zero concentration according to

$$s = s_0(1 - k_s c). \qquad \text{[IV3]}$$

Here s_0 is the sedimentation constant at infinite dilution and k_s is a proportionality constant. The results of s_0 and k_s are presented in Table I.

From s_0 and D_0 the molar mass M was calculated with

$$M = s_0 RT/D_0(1 - \bar{v}\delta_0). \qquad \text{[IV4]}$$

The partial specific volume was determined experimentally in cyclohexane, $\bar{v} = 0.621$ cm^3 g^{-1}. We assumed the same value for $\bar{v}$ in n-heptane. The values for the density of the solvent, δ_0, were taken from the literature (31). Data for M are also compiled in Table I. From the molar mass and the

number of particles

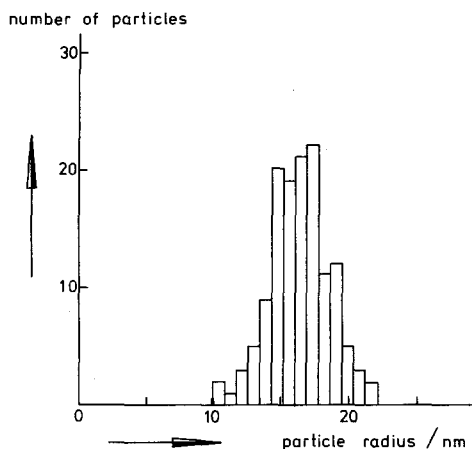FIG. 3. Size distribution of sample S_3 determined by electron microscopy. Total number of counted particles is 133.

specific volume, the radius, a_M, can also be calculated (see Table I).

The particle size distribution, $g(a)$, was determined from the Schlieren peaks of two concentrations in n-heptane ($c = 19.4$ and 6.15 g dm^{-3}). We used the method of Hermans and Ryke (32). From each concentration four peaks were measured and these "apparent distributions" were extrapolated against $(1/t)$ to infinite time (33), because the contribution of diffusion to the boundary spread is not negligible for these small particles.

The boundary sharpening effect due to particle interactions was eliminated by extrapolation to zero concentration. Applying Stokes' law, which introduces a small error since $a_D > a_M$, we find $g(a)$ from $g(s_0)$. The standard deviation is 17%, which is close to the value of 13% determined from electron microscopy.

The experimental k_s data can be compared with theoretical values for hard spheres, k_{HS}, in terms of a factor $q = \phi/c$ (see also Section VI). Assuming that the silica particles behave hydrodynamically as hard spheres, one may calculate q by equating $k_s = k_{HS}q$. Many values for k_{HS} have been proposed; see e.g. (34). Taking Batchelor's value (35) we obtain $q = 0.74$

cm^3 g^{-1} in n-heptane and $q = 0.67$ cm^3 g^{-1} in cyclohexane. In Section VIII we will discuss these results in comparison with the interpretation of light-scattering data.

V. STATIC LIGHT-SCATTERING EXPERIMENTS

Three static light-scattering experiments were performed; in cyclohexane with particle concentrations 0–0.8 g cm^{-3} (series A and B) and in chloroform with particle concentration 0–0.46 g cm^{-3} (series C). First the silica, which is usually stored as a concentrated solution in cyclohexane, is dried at 60–70°C for 18 hr. The sample dispersions were prepared either by diluting a concentrated stock solution in the cuvette (A and B) or by weighing and dissolving silica directly in the cuvette (C). The experimentally measured particle density was used to determine the concentration (w/v). The dispersions were thoroughly homogenized by shaking (and sometimes sonication) and prior to measurement the solutions were centrifuged at 5000 rpm for a few minutes to remove dust. The measured signal was always constant in time within ~2% even for low θ, indicating the absence of dust particles.

TABLE I

Light-Scattering Fluctuation Spectroscopy Results (Measured at 25.0°C) and Ultracentrifuge Results (Measured at 23.1–23.5°C) of Dilute Silica Dispersions in Cyclohexane, Chloroform, and n-Heptane[a,b]

	Solvent		
	Cyclo-hexane	Chloro-form	n-Heptane
η_0 (10^{-3} kg m^{-1} sec^{-1})	0.902	0.542	0.386
D_0 (10^{-11} m^2 sec^{-1})	1.10	1.88	2.45
a_D (nm)	22	21.5	23
s_0 (10^{-10} sec)	0.681[c]	—	1.81
k_s (cm^{-3} g^{-1})	4.4[c]	—	4.8
M (10^7 g mol^{-1})	2.95	—	3.17
a_M (nm)	19.4	—	19.8

[a] The sedimentation data are converted to 25.0°C.
[b] Viscosity data are taken from the literature (29).
[c] See Ref. (30).

First we shall now present some primary results, which are not yet corrected for attenuation of the incident and scattered light. Then we will treat the results (corrected if necessary) for $K \rightarrow 0$, and also results for $K > 0$. Finally we shall pay some attention to the strongly increasing scattering intensity at small θ, which is observed at very high concentrations.

1. Primary Results

Light-scattering results for low to intermediate concentrations are given for some silica dispersions at $\lambda_0 = 436$ nm: Fig. 4, series B in cyclohexane; Fig. 5, series C in chloroform. Similar results were obtained for series A and at $\lambda_0 = 546$ nm. The
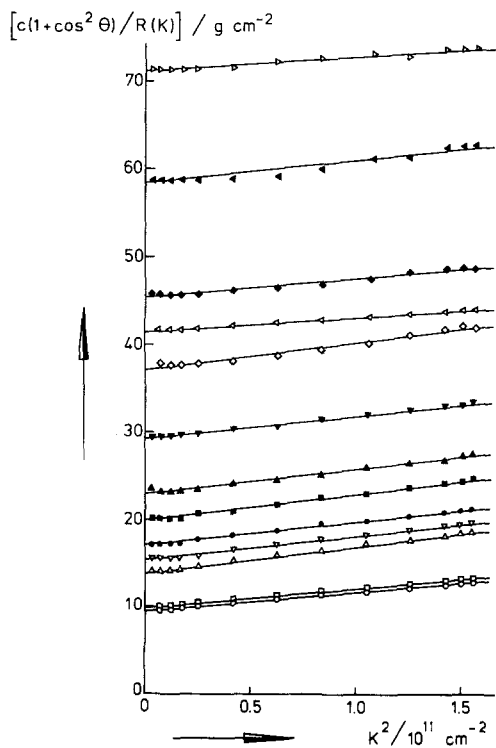

FIG. 5. Light-scattering results of series C (in chloroform), for $\lambda_0 = 436$ nm. The concentrations are in g cm^{-3}: (○) 0.00925; (●) 0.0458; (□) 0.0885; (■) 0.113; (△) 0.124; (▲) 0.200; (◆) 0.467. Also a dispersion with $c = 0.297$ was measured, but the result is not shown here for reasons of clarity.

scattering intensity in chloroform is much smaller than in cyclohexane. This must be attributed to the closer proximity of the refractive index of particles and solvent in chloroform. The angular dependence of the scattering is simply linear in K^2. In chloroform there is a curvature at small angles, shown in Fig. 5 (which is plotted on a logarithmic scale because of the curvature). This is probably caused by polydispersity in size and optical density of the particles which is more perceptible in chloroform because of nearly matching refractive indices. This is discussed in more detail elsewhere (36).

In the range of intermediate to high silica concentration, increasing deviations from the simple, linear K^2-dependence were found at small K values. A very pronounced forward scattering emerges which increases with increasing concentration. An example is given in Fig. 6 for series B in cyclohexane. For the larger scattering angles, however, the plots become linear again. This phenomenon is attributed to the formation of large clusters of particles. It will be discussed further in Section VII.

FIG. 4. Light-scattering results of series B (in cyclohexane), for $\lambda_0 = 436$ nm. The concentrations, c, are in g cm^{-3}: (○) 0.0089; (□) 0.0110; (△) 0.0423; (▽) 0.0540; (●) 0.0721; (■) 0.0934; (▲) 0.124; (▼) 0.153; (◇) 0.191; (◁) 0.192; (◆) 0.217; (◀) 0.254; (▷) 0.276.
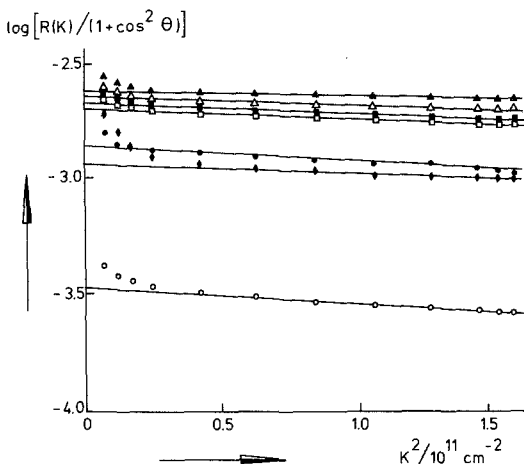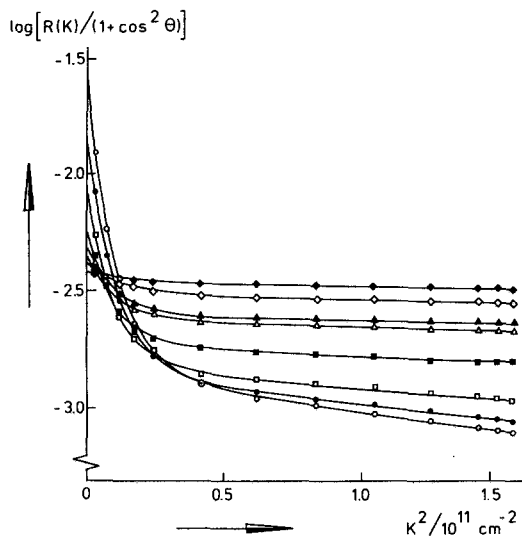
$\log\left[R(K)/(1+\cos^2\theta)\right]$

FIG. 6. Idem Fig. 4. The concentrations are in g cm^{-3}: (O) 0.809; (●) 0.728; (□) 0.664; (■) 0.576; (△) 0.461; (▲) 0.460; (◇) 0.390; (◆) 0.351.

2. Scattering at $K \to 0$

The scattering intensity in the long-wavelength limit $K \to 0$ is found by extrapolation from finite angles. For the lower and intermediate concentrations this extrapolation can be accurately performed, because of the linearity of the plots (see Fig. 4 for cyclohexane). For chloroform,

points below $\theta = 60°$ were omitted (see previous section).

Results for the lowest concentrations are presented separately in Fig. 7. According to Eq. [II9], M and A_2 can be calculated. Because the refractive index increment could not be determined accurately, we have calculated instead the refractive index of the particles from the M value as determined by sedimentation velocity and diffusion (see Table II). Values of A_2 could only be estimated and are given in Table II. For a more extended concentration range including the intermediate concentrations the extrapolated intensities were expressed as $\partial\Pi/\partial\rho$ according to Eq. [II8] after a proper normalization of $\partial\Pi/k_BT\partial\rho$ to unity at $\rho \to 0$. The uncertainty in this normalization introduces a systematic error in $\partial\Pi/\partial\rho$ which is less than 10%. Results for series A ($c = 0$–0.5 g cm^{-3}), series B ($c = 0$–0.35 g cm^{-3}), and series C ($c = 0$–0.30 g cm^{-3}) are shown in Fig. 8 for $\lambda_0 = 436$ nm. The square root of $\partial\Pi/k_BT\partial\rho$ is taken in view of the large range of values this quantity assumes. The results for $\lambda_0 = 546$ nm (not shown for clarity) are in good agreement with those for $\lambda_0 = 436$ nm.

For the highest concentrations extrapola-

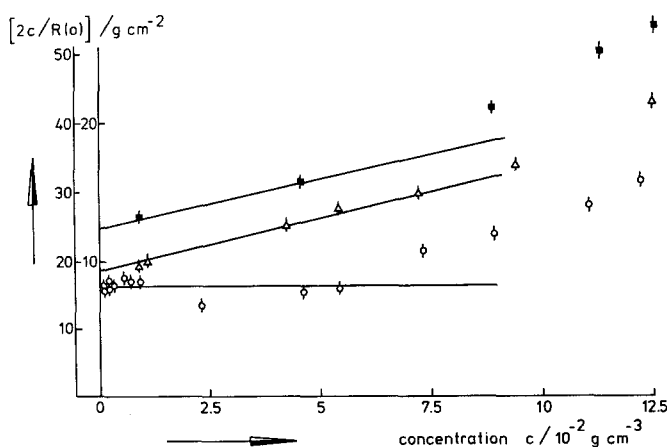
FIG. 7. Zero angle scattering as a function of particle concentration in the dilute region ($\lambda_0 = 436$ nm). The left-hand ordinate scale corresponds with series C (■), the right-hand one to series A (O), and series B (△). The factor 2 in $[2c/R(0)]$ originates from the $(1 + \cos^2 \theta)$ term.

tion to $K = 0$ is very difficult, due to the strong curvature in the angular dependence at small θ (see Fig. 6). Some data for series B are shown as vertical bars in Fig. 8. They show a discontinuity with the trend at intermediate concentrations. The relative decrease in $\partial\Pi/\partial\rho$ is attributed by us to the presence of large clusters of particles. The angular dependence at higher angles is still linear in K^2 (see Fig. 6). One could argue that in this angular range the scattering phenomenon probes the osmotic compressibility of the particles *inside* the large clusters. To check this we extrapolated the *linear* parts of the plots ($\theta > 90°$) to $K = 0$. These extrapolated points are also given in Fig. 8. One observes indeed that the trend of the intermediate concentrations now continues smoothly to larger concentrations although there is still a downward trend at the highest concentrations.

3. Scattering at $\theta = 150°$

In view of the uncertainties introduced by the sometimes long extrapolations required to obtain the scattering at $\theta = 0$, we will also give the results for series B at $\theta = 150°$. For convenience they are also expressed as a normalized $\partial\Pi/\partial\rho$ in Fig. 8 (triangles). One notes also that these data follow a smooth curve over the whole concentration range.

TABLE II

Light-Scattering Data Obtained from Dilute Dispersions[a]

	Experiment		
	A	B	C
Δn ($\lambda_0 = 546$ nm) (10^{-2})	2.5	2.3	1.5
Δn ($\lambda_0 = 436$ nm) (10^{-2})	2.4	2.0	1.3
A_2 ($\lambda_0 = 436$ nm) (cm^3 g^{-1})	0	4	3
R_g ($\lambda_0 = 546$ nm) (nm)	27	28	29
R_g ($\lambda_0 = 436$ nm) (nm)	23	27	23

[a] Values for Δn were calculated with $M = 3.0 \times 10^7$ g mol^{-1}. The temperature ranged from 24.4 to 27.0°C. The uncertainty in Δn, A_2, and R_g is 0.001, 1 cm^3 g^{-1}, and 2 nm, respectively.
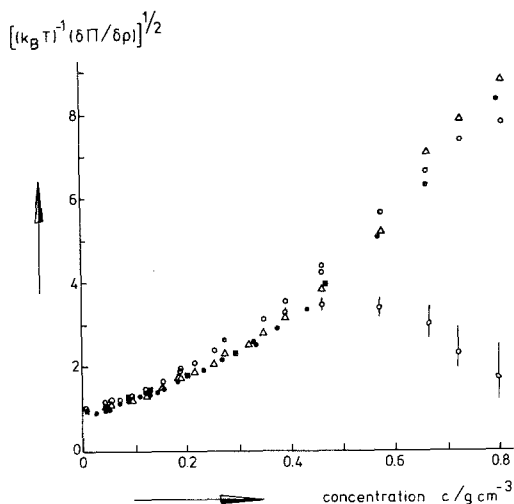
FIG. 8. The square root of $(k_BT)^{-1}(\partial\Pi/\partial\rho)$ for $\lambda_0 = 436$ nm: (●) series A; (○) series B; (■) series C; (△) series B, but instead of data extrapolated to $\theta = 0°$, data at $\theta = 150°$ are taken. Data with error bars correspond to results extrapolated to $K \to 0$ from small θ, see text.

4. Slope of the Angular Dependence as a Function of Concentration

From Fig. 6 one observes that the (limiting) slope of the curves at higher K^2 values depends on concentration. The reason is that for $c > 0$, interactions between particles also affect the angular dependence, (see Eqs. [II1], [II16]). For convenience we shall express the slope as an apparent radius of gyration $(R_g^2)_{app}$. At $c = 0$ this equals R_g^2 of the particles (see Table II). The variation of $(R_g^2)_{app}$ with concentration is plotted in Fig. 9. Because the angular dependence is small, the apparent radius of gyration cannot be determined very accurately. We estimate the accuracy in Fig. 9 to be ~100 nm^2. For the sake of clarity error bars are not drawn in the figure. The results for $\lambda_0 = 546$ nm exhibit the same trend. The absolute values, however, mostly exceed the 436-nm results, the largest discrepancy being 300 nm^2 and generally <150 nm^2. We have no explanation for this discrepancy. For both wavelengths the apparent radius of gyration of series B
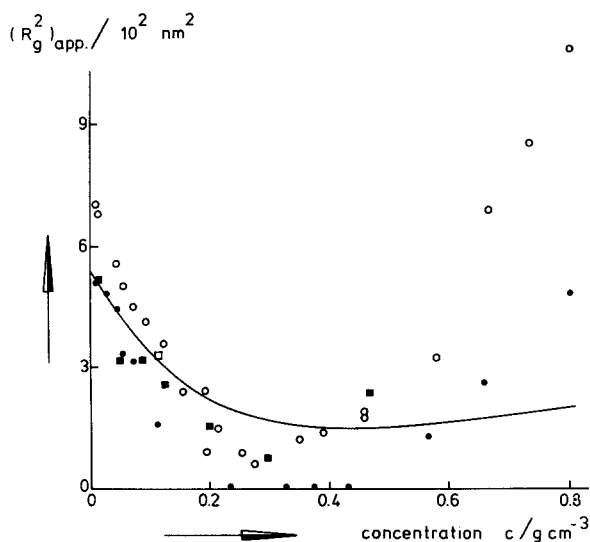
FIG. 9. The apparent radius of gyration as a function of concentration ($\lambda_0 = 436$ nm); ($\bullet$) series A; ($\bigcirc$) series B; ($\blacksquare$) series C. The drawn line is a theoretical curve (see Section VI).

slightly exceeds the values for A and C. This will be discussed in Section VIII.

VI. INTERPRETATION WITH FLUID-STATE THEORIES

The experimental $\partial\Pi/k_B T\partial\rho$ data can be compared with theoretical results, e.g., Eq. [II18], when the volume fraction is known. However, since $\partial\Pi/\partial\rho$ is strongly dependent on ϕ, the specific volume of interaction, q, which relates the experimental concentration to the volume fraction ($\phi = qc$), should be known very accurately. Therefore it is more appropriate to treat q as the fitting parameter. Then from q the hard-sphere diameter, σ, can be calculated quite accurately since

$$\sigma = [6qM/\pi N_A]^{1/3}. \qquad [VI1]$$

We will now discuss the compressibility, the position and numerical value of the maximum of $R(0)$, the structure factor at $\theta = 150°$, and the angular dependence as a function of concentration.

1. Reciprocal Compressibility

The experimental compressibility data (see Fig. 8) were fitted with Eq. [II18]. In

Fig. 10 such a fit is shown for series A ($0 \leq \phi \leq 0.3$) with $q = 0.73$ cm^3 g^{-1}. The error in q arising from the systematic error in $\partial\Pi/\partial\rho$ ($<10\%$) is 0.03 cm^3 g^{-1}. The random error in $\partial\Pi/\partial\rho$ is mainly due to the $K \rightarrow 0$ extrapolation and is smaller than 5%. One notes from Fig. 10 that except for the lower concentrations the experimental data are close to the theoretical curve. Clearly the interactions can be reasonably described with the hard-sphere model. For series C we obtained a good fit for $q = 0.75 \pm 0.03$ cm^3 g^{-1}. Also for series B the results could be fitted quite well, but with $q = 0.87 \pm 0.04$ cm^3 g^{-1}, which is significantly larger than for A and C. This will be discussed in Section VIII. The experimental data can be fitted equally well with a theoretical curve, which has been corrected for the polydispersity of the sample (see Eq. [II21]. Slightly larger q values were obtained for each series (see Table III).

q can be determined rather accurately at $0.1 < \phi < 0.4$, because $\partial\Pi/\partial\rho$ increases steeply with ϕ in this region. At $\phi < 0.1$, however, q is inaccurate, since $\partial\Pi/\partial\rho$ is less steeply increasing with ϕ and also the
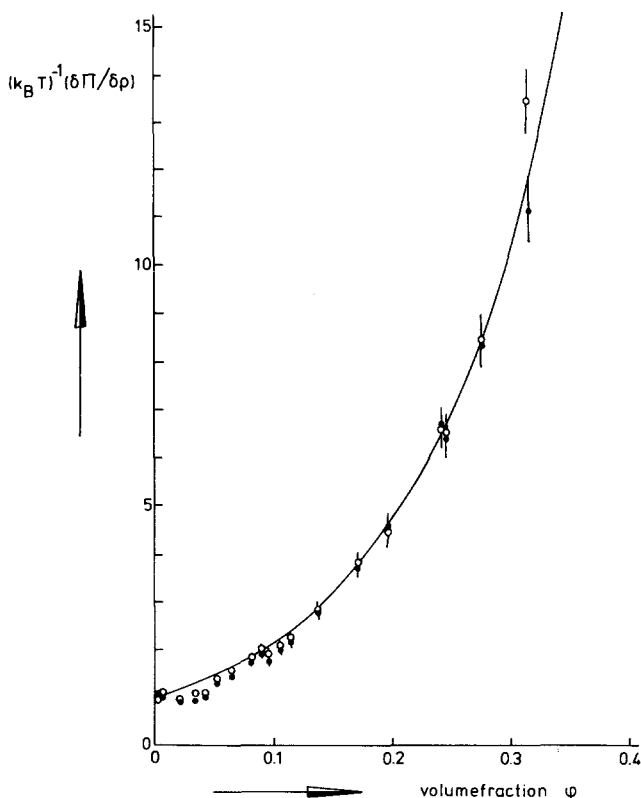
FIG. 10. Comparison of experimental and theoretical (drawn line) $(k_B T)^{-1}(\partial\Pi/\partial\rho)$ as a function of the volume fraction (series A). ($\bigcirc$) $\lambda_0 = 546$ nm; ($\bullet$) $\lambda_0 = 436$ nm; q = 0.73 cm³ g⁻¹.

experimental data are scattered. Estimates of q $(=A_2/4$; compare Eqs. [II9] and [II19]) determined at low concentrations are also given in Table III.

A more sensitive test is possible by plotting $[(k_B T)^{-1}(\partial\Pi/\partial\rho)(1 - \phi)^4]^{1/2}$ versus ϕ $(=qc)$, similar to Fig. 1. In Fig. 11 the results of such a comparison are shown for $q = 0.73$ cm³ g⁻¹ (series A), $q = 0.87$ cm³ g⁻¹ (series B), and $q = 0.75$ cm³ g⁻¹ (series C). Errors in the data of Fig. 11 are estimated from the systematic error in the experimental $(\partial\Pi/\partial\rho)$ values and their corresponding error in q values. The error in c is negligible. Error bars are drawn for the result of series C. Series C shows an excellent fit up to $\phi = 0.35$. Series A and B show deviations at $\phi > 0.4$. This will be discussed in Section VIII.

*2. Maximum in the Scattering
Intensity R(0)*

Recalling Eqs. [II8], [II18], and [II23] one can derive for $R(0)$

$$qR(0)/2\mathcal{K}M = \phi(1 - \phi)^4[(1 + 2\phi)^2$$
$$+ \phi^3(\phi - 4) - \epsilon\phi(1 - \phi)^4]^{-1}. \quad [VI2]$$

This equation shows a maximum of $R(0)$ at a certain $\phi = \phi_{max} = 0.1304$. The position of ϕ_{max} does not depend on ϵ. The height of the maximum is 0.0472 for hard spheres ($\epsilon = 0$) and becomes larger for $\epsilon > 0$.

From the position of the maximum one may obtain a value of $q = 0.1304/c_{max}$. Because the maximum is not very sharp and the experimental data are scattered, q can only be estimated roughly (see Table III). For series C the height of the maximum compares well with the theoretical hard-

TABLE III

q Values (cm^3 g^{-1}) Obtained by Comparing the Theoretical Carnahan–Starling Equation with Experimental Data

	Series		
	A	B	C
$0 < \phi < 0.10$	0 ± 0.4	1.0 ± 0.25	0.75 ± 0.25
$0 < \phi < 0.40$	0.73 ± 0.03	0.87 ± 0.04	0.75 ± 0.03
$0 < \phi < 0.40^a$	0.76 ± 0.03	0.91 ± 0.04	0.78 ± 0.03
$\phi = 0.1304^b$	0.9 ± 0.1	1.0 ± 0.1	0.65 ± 0.1

^{a} Polydispersity taken into account in the theoretical equation.
^{b} Turbidity maximum.

sphere value. For series A and to a minor extent also for B the maximum is higher.

3. Structure Factor at $\theta = 150°$

The experimental $[S(K)]^{-1}$ values, which were determined for K corresponding to $\theta = 150°$ (see Fig. 8), can also be fitted with theoretical values. In this way we obtain a check on the consistency of the fitting procedure at $K = 0$ and $K > 0$. The theoretical curve was calculated according to Eqs. [II16] and [II17]. For A and B we calculated σ from q and M according to Eq. [VI1]. The error due to truncation at the K^2-term was less than 2%. It appeared that a similar

fit as in Fig. 11 could be obtained, indicating that the experimental results at $\theta = 150°$ can be fitted with the theoretical result, using the q values obtained at $K = 0$.

4. Apparent Radius of Gyration

By combining Eqs. [II1], [II4], [II16], and [II17] we obtain for the apparent radius of gyration

$$(R_g^2)_{\text{app}} = R_g^2 - 3\sigma^2[(4\phi/5) - (11\phi^2/20)$$
$$+ (\phi^3/5)](1 + 2\phi)^{-2}. \quad \text{[VI3]}$$

The decrease in the apparent radius of gyration due to the hard-sphere interaction can be calculated when σ is known. If we take $q = 0.73$ cm^3 g^{-1} and $\sigma = 41.1$ nm, the second term in the right-hand side of Eq. [VI3] can be determined (solid line in Fig. 9). The theoretical curve (with $R_g^2 = 5.4 \times 10^2$ nm^2) yields qualitatively the same picture as the experimental points. The most remarkable discrepancy is the more pronounced increase at very high concentrations.

VII. CLUSTER FORMATION

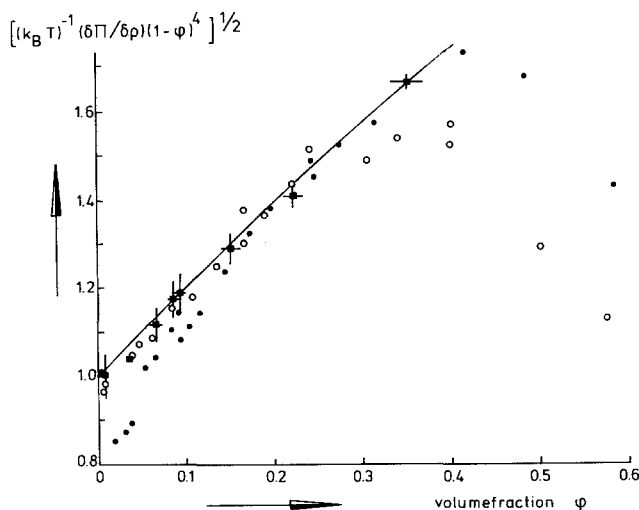For the highest dispersion concentrations in cyclohexane and also to some extent in

FIG. 11. Fit of theoretical CS equation (drawn line) and experimental results ($\lambda_0 = 436$ nm); ($\bullet$) series A, $q = 0.73$ cm^3 g^{-1}; ($\bigcirc$) series B, $q = 0.87$ cm^3 g^{-1}; ($\blacksquare$) series C, $q = 0.75$ cm^3 g^{-1}.

chloroform, we found a strongly upward bending scattering curve at small angles (see Figs. 5 and 6). In this section we will go into a little more detail on this phenomenon. The basic idea is that at high concentrations a small number of large clusters of particles is formed. This cluster formation is probably reversible, because it disappears upon dilution with solvent. Perhaps it may be correlated with a phase transformation from the liquid to an ordered state. For the scattering of such a system we shall write analogous to Eq. [III1] (see e.g. (37))

$$R'(K)/(1 + \cos^2 \theta) = \mathcal{K}cMP(K)S(K)$$
$$+ \mathcal{K}'c'M'P'(K)S'(K), \quad [VII1]$$

where the second term of the right-hand side denotes the contribution of clusters. $R'(K)$ is the scattering of the total system (i.e., individual particles + large clusters), which is experimentally measured. The symbol $R(K)$ in the previous sections was used to designate the scattering of the individual particles (with maybe some doublets), which can be measured directly at high θ, because $P'(K)$ falls off very rapidly with θ and the presence of clusters is probably not observed anymore at $\theta > 90°$. At low angles the size of the clusters is detected and at high angles the interior of the clusters determines the scattering. For low θ, $R(K)$ is found by extrapolation. If we now assume that the mutual interaction between clusters is small, $S'(K) \simeq 1$, then the size of the clusters can be determined from the difference of $R'(K)$ minus $R(K)$ according to

$$[R'(K) - R(K)]/(1 + \cos^2 \theta)$$
$$= \mathcal{K}'c'M'P'(K). \quad [VII2]$$

For both wavelengths we found for the radius of the cluster $a' \simeq 200$ nm (Fig. 12). Also a rough estimate can be made of the concentration of clusters from the difference $R'(0) - R(0)$. From Eq. [VII2] we get for $K = 0$ by dividing with $R(0)$
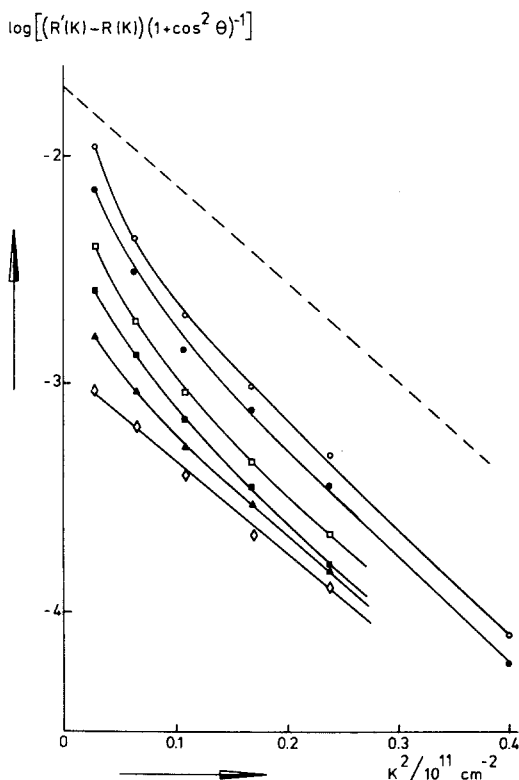

FIG. 12. The angular dependence of scattered light (experiment B, $\lambda_0 = 436$ nm), corrected by subtracting $R(K)$, which is found by extrapolation from higher θ. The concentrations are in g cm^{-3}: (○) 0.809; (●) 0.728; (□) 0.664; (■) 0.576; (▲) 0.460; (◇) 0.390. The dashed line represents $P'(K)$ of a cluster with radius 210 nm.

$$[R'(0) - R(0)]/R(0)$$
$$= (dn/dc')^2c'M'/(dn/dc)^2cMS(0), \quad [VII3]$$

where (dn/dc') is the refractive index increment of the cluster, which is not equal to (dn/dc), because the scattering power of the cluster is determined by the difference of the refractive indices of cluster, n', and concentrated solution of individual particles, n, $(dn/dc') = (n' - n)/\delta'$, δ' is the density of the cluster. For n', n, and δ' we have

$$n' = n_0 + (dn/dc)c_c,$$
$$n = n_0 + (dn/dc)c,$$
$$\delta' = \phi_c\delta + (1 - \phi_c)\delta_0. \quad [VII4]$$

TABLE IV

Estimates of Cluster Concentration c'/c
for Experiment B, $\lambda_0 = 546$ nm

Concentration (g cm^{-3})	$[c'/c]$ (10^{-2})
0.81	>2
0.73	1
0.66	0.4
0.58	0.2
0.46	0.07
0.39	0.03

Here c_c and ϕ_c are the concentration and volume fraction of particles in the cluster. δ_0 is the density of the solvent. From Eq. [VII4] we obtain for the ratio of refractive index increments

$$(dn/dc')/(dn/dc)$$

$$= (c_c - c)/[\phi_c\delta + (1 - \phi_c)\delta_0]. \quad [VII5]$$

This ratio can be calculated taking $\delta = 1.61$, $\delta_0 = 0.774$ g cm^{-3}, and $\phi_c = 0.637$, which is found for dense packings of hard spheres (38). From the size we can estimate the ratio M'/M and then also the ratio c'/c can be determined. In Table IV some values are listed for experiment B, $\lambda_0 = 546$ nm. The concentration of large clusters appears to be quite low even at the highest concentrations. If $S'(0) < 1$ Eqs. [VII2] and [VII3] are not valid and the calculated concentration of large clusters would be larger.

VIII. DISCUSSION

1. Concentrated Dispersions

From Figs. 10 and 11 we note that the experimental $\partial\Pi/\partial\rho$ data can be fitted in a large range of volume fractions with a single q value. This indicates that the hard sphere is a good model for particle–particle interactions in these dispersions. One cannot judge the importance of polydispersity or nonsphericity, however, because theoretical results, which take these effects into account, can be equally well fitted with slightly different q values. Series C in

chloroform shows an excellent fit for all volume fractions, corresponding to $0 < c < 0.46$ g cm^{-3}. Series A and B in cyclohexane also show a reasonable fit for $\phi < 0.4$. In series A, however, the low A_2 and sharper maximum of $R(0)$ vs c seem to indicate some attraction. The fitting procedure of the structure factor at $\theta = 150°$ yields consistent results with $\partial\Pi/\partial\rho$.

In discussing q values (see Table III), we will focus on the data obtained with the fit at $0 < \phi < 0.4$ (without polydispersity correction), because these values are more accurate than the values obtained from A_2 and c_{max}. q can be determined most accurately from experimental data at $0.1 < \phi < 0.4$. Within experimental error A and C are in good agreement. The q value of series B is larger. Because in series B the experimental data also fit the theoretical equation, the quality of the fit itself is not a satisfactory criterion for choosing the correct q. We think that the q value of A and C is better, because it is close(r) to the value determined from sedimentation in n-heptane and cyclohexane and also to the experimentally measured specific volume ($=0.621$ cm^3 g^{-1}, see Section IV). Therefore we calculated the distance of hard-sphere interaction, $a_{HS} = \sigma/2$, from q obtained for A. From Eq. [VI1] we obtained $a_{HS} = 20.6 \pm 0.4$ nm (see Table V) which is quite comparable with a_D and a_M. In the next subsection we will discuss the results of B.

2. Complications

Contrary to the interpretation of the results for $\phi < 0.4$ complications due to cluster formation arise for $\phi > 0.4$. Large clusters cause strongly upward bending scattering curves (see Figs. 5 and 6), which make extrapolation to $K \to 0$ very difficult. Consequently the compressibility of the particles inside the clusters can only be roughly estimated by extrapolation from $\theta \geqslant 90°$. Presumably the less steeply increasing

$\partial\Pi/\partial\rho$ (Fig. 8), the increase in $(R_g^2)_{app}$ (Fig. 9), and the deviation from the theoretical curve (Fig. 11) all at high ϕ stem from erroneous extrapolation.

We investigated whether or not the large q value of series B could be correlated with the occurrence of small aggregates of particles, e.g., doublets. Using the q value *of series A* in order to calculate ϕ, $[(k_BT)^{-1}(\partial\Pi/\partial\rho)(1 - \phi)^4]^{1/2}$ was plotted vs ϕ (see Fig. 13) analogous to Fig. 11. The dots show an approximately linear increase with ϕ with a slope of 2.8. The dashed line represents the hard-sphere theoretical curve, as given in Fig. 11 with a slope of approximately 2.

The value 2.8 is intermediate between 2.0 (hard spheres) and 3.8 (hard dumbbells); see Fig. 1.

Another indication for the presence of doublets is $R_g(a_{R_g})$, which is high compared to a_D (see Tables II and V). Nonhomogeneity of the optical density within the particle can be important in chloroform but not in cyclohexane (36). Neither could nonsphericity explain the discrepancy, since R_g (6) and D_0 (39) are affected qualitatively in the same manner. For systems with doublets and triplets of particles Benoit *et al.* (40) derived

$$R(K)/\mathscr{K}cM = (1 + P + 4Q/3 + \cdots)$$
$$- (Ka_{R_g})^2(1 + 13P/3$$
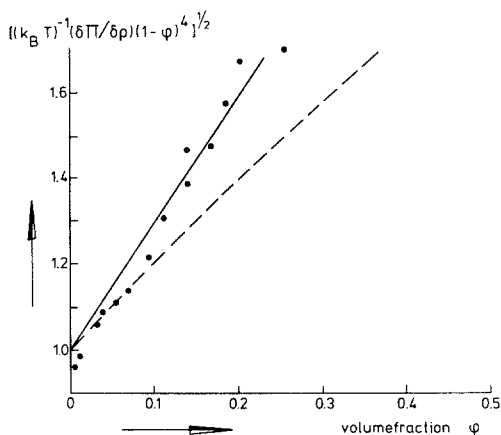$$+ 112Q/9 + \cdots)/5, \quad [VIII1]$$

where $P = c_2/c$ and $Q = c_3/c$, c, c_2, and

FIG. 13. Fit of experimental results of series B ($\lambda_0 = 436$ nm) for $q = 0.73$ cm^3 g^{-1}. The experimental points are markedly higher than the theoretical CS result (-----).

c_3 being the total, doublet, and (linear) triplet concentrations (w/v), respectively. The difference between a_{R_g} and a_D can be explained by taking, e.g., $P = 0.2$ and $Q = 0$, or $P = 0.1$ and $Q = 0.05$. The light-scattering fluctuation spectroscopy technique is much less sensitive to the presence of doublets. The presence of, e.g., 20% doublets affects the hydrodynamic radius only to a minor extent. From the translational friction coefficients of doublets and triplets (41), the sedimentation constants can also be calculated.

No significant shoulders, however, were found in the sedimentation experiments, indicating that the amount of doublets etc. is small. We conclude that some doublets and/or triplets offer a satisfactory explanation for the large R_g. Comparing R_g values of series A and B it seems that more doublets are present in series B.

The differences in series A and B presumably originate from the preparation procedure, which was different for both series. It is conceivable that the centrifugation, which was carried out three times for series B in order to remove excess stearyl alcohol, caused the formation of aggregates which did not completely disperse again.

TABLE V

The Particle Size (in nm) (Measured with Different Techniques) and Distance of Hard-Sphere Interaction (in nm) for the Experiments in Cyclohexane

a_{EM}	a_D	a_M	$a_{R_g}{}^a$	$a_{HS}{}^b$
16.5	22 ± 1	19.4 ± 0.2	30 ± 3	20.6 ± 0.4

[a] Calculated from $a_{R_g} = (5/3)^{1/2}R_g$ for $R_g = 23 \pm 2$ nm.

[b] Calculated with $q = 0.73 \pm 0.03$ cm^3 g^{-1}, $M = 3.0 \pm 0.1 \times 10^7$ g mol^{-1}.

3. Conclusions

Organophilic silica appears to be a proper model colloid to study particle–particle interactions in apolar media in a large range of concentrations. Fluid-state theories can be successfully applied to interpret light-scattering results of concentrated silica dispersions in cyclohexane and chloroform. Compressibilities and also scattering results at $\theta = 150°$ agree rather well with the hard-sphere model. Large clusters of particles appear at the highest concentrations. Small aggregates (e.g., doublets) are sometimes present at all concentrations.

REFERENCES

1. Brown, J. C., Pusey, P. N., Goodwin, J. W., and Ottewill, R. H., *J. Phys. A Math. Nucl. Gen.* **8**, 644 (1975); Brown, J. C., Goodwin, J. W., Ottewill, R. H., and Pusey, P. N., in "Colloid and Interface Science" (M. Kerker, Ed.), Vol. 4, p. 59. Academic Press, New York, 1976.
2. Van Megen, W., and Snook, I., *J. Chem. Phys.* **66**, 813 (1977).
3. Vrij, A., Nieuwenhuis, E. A., Fijnaut, H. M., and Agterof, W. G. M., *Faraday Discuss. Chem. Soc.* **65**, 101 (1978); Nieuwenhuis, E. A., and Vrij, A., *J. Colloid Interface Sci.* **72**, 321 (1979).
4. Agterof, W. G. M., Van Zomeren, J. A. J., and Vrij, A., *Chem. Phys. Lett.* **43**, 363 (1976).
5. Ross, P. D., and Minton, P., *J. Mol. Biol.* **112**, 437 (1977).
6. Kerker, M., "The Scattering of Light and Other Electromagnetic Radiation." Academic Press, New York, 1969.
7. Guinier, A., and Fournet, G., "Small Angle Scattering of X-Rays," p. 126. Wiley, New York, 1955.
8. Croxton, C., "Introduction to Liquid State Physics." Wiley, London, 1975.
9. Ornstein, L. S., and Zernike, F., *Proc. Acad. Sci. (Amsterdam)* **17**, 793 (1914).
10. Alder, B. J., and Wainwright, T. E., *J. Chem. Phys.* **33**, 1439 (1960).
11. Percus, J. K., and Yevick, G. J., *Phys. Rev.* **110**, 1 (1958).
12. Thiele, E., *J. Chem. Phys.* **39**, 474 (1963); Wertheim, M. S., *Phys. Rev. Lett.* **10**, 321 (1963).
13. Carnahan, N. F., and Starling, K. E., *J. Chem. Phys.* **51**, 635 (1969).
14. Sharma, R. V., and Sharma, K. C., *Physica* **89A**, 213 (1977).
15. Reiss, H., Frisch, H., and Lebowitz, J. L., *J. Chem. Phys.* **31**, 369 (1959).
16. Gibbons, R. M., *Mol. Phys.* **17**, 81 (1969).
17. Nezbeda, I., *Mol. Phys.* **33**, 1287 (1977).
18. Boublik, T., *J. Chem. Phys.* **63**, 4084 (1975).
19. Few, G. A., and Rigby, M., *Chem. Phys. Lett.* **20**, 433 (1973); Monson, P. A., and Rigby, M., *Mol. Phys.* **35**, 1337 (1978).
20. Freasier, B. C., Jolly, D., and Bearman, R. J., *Mol. Phys.* **31**, 255 (1976).
21. Vrij, A., *J. Chem. Phys.* **69**, 1742 (1978); **71**, 3267 (1979).
22. Isihara, A., and Hayashida, T., *J. Phys. Soc. Japan* **6**, 46 (1951).
23. Kihara, T., *J. Phys. Soc. Japan* **8**, 686 (1953).
24. Stöber, W., Fink, A., and Bohn, E., *J. Colloid Interface Sci.* **26**, 62 (1968).
25. Iler, R. K., U. S. Patent, 2,801,185.
26. Van Helden, A. K., Jansen, J. W. J., and Vrij, A., *J. Colloid Interface Sci.*, submitted.
27. Putzeys, P., and Dory, E., *Ann. Soc. Sci. Bruxelles Ser. 1* **60**, 37 (1940).
28. Berne, B. J., and Pecora, R., "Dynamic Light Scattering." Wiley, New York, 1976.
29. Weast, R. C. (ed), "Handbook of Chemistry and Physics," 53rd ed. Chem. Rubber Co., Cleveland.
30. Kops-Werkhoven, M., and Fijnaut, H. M., to be published.
31. Johnson, B. L., and Smith, J., in "Light Scattering from Polymer Solutions" (M. D. Huglin, Ed.). Academic Press, London, 1972.
32. Hermans, J. J., and Ryke, A. M., *J. Colloid Sci.* **13**, 508 (1958).
33. Baldwin, R. L., *J. Amer. Chem. Soc.* **76**, 402 (1954).
34. Altenberger, A. R., *J. Chem. Phys.* **70**, 1994 (1979).
35. Batchelor, G. K., *J. Fluid Mech.* **52**, part 2, 245 (1972).
36. Van Helden, A. K., and Vrij, A., *J. Colloid Interface Sci.* **76**, 418 (1980).
37. Huijben, M. J., thesis, p. 184, University of Groningen, 1978.
38. Cargill, G. S., *J. Appl. Phys.* **41**, 2248 (1970).
39. Perrin, J., *J. Phys. Radium* **7**, 1 (1936).
40. Benoit, H., Ullman, R., De Vries, A. J., and Wippler, C., *J. Chim. Phys.* **59**, 889 (1962).
41. Kirkwood, J. G., *J. Polym. Sci.* **12**, 1 (1954).